Available online at www.sciencedirect.com
SCIENCE DIRECT
International Journal of Heat and Fluid Flow 27 (2006) 336–347
International Journal of HEAT AND FLUID FLOW
www.elsevier.com/locate/ijhff

Flow structure in the near-field of buoyant low-density gas jets

Rajani P. Satti [a], Ajay K. Agrawal [b,*,1]

[a] School of Aerospace and Mechanical Engineering, University of Oklahoma, Norman, OK 73019, United States
[b] Department of Mechanical Engineering, University of Alabama, Tuscaloosa, AL 35487, United States

Received 22 June 2005; accepted 15 October 2005
Available online 13 December 2005

Abstract

Flow structure of helium jets injected into quiescent air was investigated numerically using finite volume approach. The analysis is based on unsteady, laminar, axisymmetric, isothermal flow in a binary fluid system. The jet Reynolds number, *Re* was varied from 40 to 150 to encompass steady and oscillating jet flow regimes. Comparison with experimental data revealed excellent agreement, proving reliability of the model in predicting global flow characteristics. At low jet Reynolds numbers, the flow was steady and the concentration shear layer at the tube exit was stratified by mixing between jet and ambient fluids inside the tube. At higher jet Reynolds numbers ($Re = 90$ and 150), buoyancy induced acceleration contracted the jet core to form a toroidal vortex by entrainment of the ambient fluid. Structural details of the globally unstable flow are discussed using instantaneous, mean and RMS profiles of helium concentration and axial velocity.

Keywords: Jets; Flow structure; Instability; Entrainment

1. Introduction

The flow structure and stability of jets has been a subject of research in various applications. Of particular interest is the low-density gas jet injected into high-density ambient with relevance to fuel leaks, engine exhaust, diffusion flames, materials processing, and natural phenomena such as fires and volcanic eruptions. Several past studies (Fay, 1973; Rodi, 1982; List, 1982; Papanicolaou and List, 1988; Lai, 1984; Dai et al., 1994; Dehmani et al., 1996; Richards and Pitts, 1993; Panchapakesan and Lumley, 1993) have described the fully turbulent far-field region of the jet, where the velocity and concentration fields achieve self-similarity. The flow structure in the far-field is however influenced by the near-field processes such as diffusion, buoyancy, entrainment, jet instability, and transition from laminar to turbulent flow. The present study focuses on the near-field flow structure of low-density gas jets injected into high-density ambient, whereby the effects of buoyancy are significant.

Pera and Gebhart (1963), Tenner and Gebhart (1971), Gebhart (1973) and Mollendorf and Gebhart (1973) studied flow instabilities and transition to turbulence in buoyant plumes and jets. They found that a laminar, buoyant water jet injected from a circular tube into a quiescent medium induced a toroidal vortex. Hamins et al. (1992) identified self-excited periodic oscillations in helium jets injected into air, and reported that a minimum jet exit velocity was required to initiate oscillations. A comprehensive insight into the flow behavior of low-density gas jets was provided by Subbarao and Cantwell (1992) using helium injected from a tube into a co-flow of air. Experiments revealed highly periodic oscillations in the near-field for a range of jet Reynolds numbers, $Re = 300$–1500 and jet Richardson numbers, $Ri = 0.5$–6.0. They speculated that the perturbations in the air stream, for example, on the surface boundary layer outside the jet tube, dominated the instability and transition from laminar to turbulent flow.

* Corresponding author. Tel.: +1 205 348 4964; fax: +1 205 348 6419.
E-mail address: aagrawal@coe.eng.ua.edu (A.K. Agrawal).
[1] Professor and Robert F. Barfield Chair of Mechanical Engineering.

0142-727X/$ - see front matter © 2005 Elsevier Inc. All rights reserved.
doi:10.1016/j.ijheatfluidflow.2005.10.012

Nomenclature

d	tube inside diameter (mm)
D_b	mass diffusion coefficient (m^2/s)
f	frequency (Hz)
g	acceleration due to gravity (m/s^2)
r	radial coordinate
Re	jet Reynolds number, $Re = U_j d/\nu_j$
Ri	jet Richardson number, $Ri = gd(\rho_\infty - \rho)/\rho U_j^2$
St	jet Strouhal number, $St = fd/U_j$
U_j	average jet exit velocity (m/s)
v_r	radial component of velocity (m/s)
v_z	axial component of velocity (m/s)
Y	mole fraction
z	axial coordinate

Greek symbols

μ	dynamic viscosity of jet fluid (kg m/s)
ν_j	kinematic viscosity of jet fluid (m^2/s)
ρ_j	density of jet fluid (kg/m^3)
ρ_∞	density of ambient fluid (kg/m^3)

Cetegen and co-workers (1993, 1996, 1997a,b) performed detailed experiments involving planar and axisymmetric plumes of helium or helium–air mixtures for a range of injector diameters, jet fluid densities, and jet exit velocities. They found that the flow oscillation frequency represented by the Strouhal number (St) correlated with Ri, suggesting that the oscillations were buoyancy induced. Velocity measurements revealed buoyant acceleration of the low-density fluid causing the jet core to contract, and thus, entrain the ambient fluid. Entrainment resulted in the formation of a toroidal vortex that interacted with the jet core while convecting downstream. Pasumarthi and Agrawal (2003) obtained instantaneous concentration measurements across the whole field using quantitative rainbow schlieren deflectometry to characterize the toroidal vortex and its interactions with the jet core. Yep et al. (2003) conducted experiments in drop tower to show that the flow oscillations occurring in Earth gravity disappeared in microgravity. These experiments provided direct evidence that the self-excited periodic oscillations in low-density gas jets are buoyancy induced.

The experimental observations have also been supported by numerical simulations of Mell et al. (1996), who achieved good agreement between computed and measured flow oscillation frequencies. The computational study by Soteriou et al. (2002) provided flow structure details of planar low-density gas jets. The nature of the instability and relative roles of buoyancy and diffusion in triggering/sustaining the instability were also explored. Using intuitive arguments, they proposed that diffusion was important in initiating the flow instability. Diffusion however assumed a secondary role after the instability was manifested.

In spite of the vast literature on jet flows, the detailed flow structure in the near-field of low-density buoyant jets has not been documented in past studies. Experimental studies have described the flow using either velocity or concentration measurements, which are inadequate to elucidate the strong coupling between velocity and concentration fields in low-density gas jets. In this regard, the analysis based on computational fluid dynamics (CFD) is useful because it provides flow structure details including simultaneous visualization of vector–scalar fields throughout the region of interest. However, past computational studies have considered either the global features of the oscillating jet (Mell et al., 1996) or the planar jets (Soteriou et al., 2002). Detailed CFD analysis is therefore needed to not only characterize the flow structure of steady and oscillating jets, but also to explain the mechanism of instability in circular jets.

The objective of the present computational study is to examine the flow structure of low-density buoyant gas jets issued from a circular tube into quiescent ambient, which is among the most practical jet configurations. Numerical simulations were performed to identify and explain interactions among velocity and concentration fields over a range of jet Reynolds numbers. Computations were done using an unsteady model and no external perturbations were introduced to ensure that the flow oscillations, if present, were self-excited. The jet flow is characterized by velocity vectors, and profiles of jet half radius, axial velocity and helium concentration, etc. Both instantaneous and mean structure is presented in case of the oscillating flow. Results are presented to highlight unique features of steady and oscillating low-density gas jets. Besides providing details of the flow structure, the mechanism of instability is explored.

2. Technical approach

2.1. Model assumptions

Experiments have shown that a round helium jet injected into air remains symmetric in the near-field region (Pasumarthi and Agrawal, 2003; Yep et al., 2003). Moreover, the flow symmetry is preserved even in the presence of unsteady effects such as the periodic oscillations. Consistent with these experimental observations, the present analysis utilizes conservation equations for unsteady, laminar, isothermal, axisymmetric flow. The air is treated as a single species to result in a binary fluid system.

2.2. Governing equations

The conservation equations of mixture mass and momentum, and species concentration are expressed as follows:

$$\frac{\partial \rho}{\partial t}+\frac{\partial}{\partial z}(\rho v_z)+\frac{\partial}{\partial r}(\rho v_r)+\frac{\rho v_r}{r}=0 \quad (1)$$

$$\frac{\partial}{\partial t}(\rho v_z)+\frac{1}{r}\frac{\partial}{\partial z}(r\rho v_z v_z)+\frac{1}{r}\frac{\partial}{\partial r}(r\rho v_r v_z) = -\frac{\partial p}{\partial z}+\frac{1}{r}\frac{\partial}{\partial z}\left[r\mu\left(2\frac{\partial v_z}{\partial z}-\frac{2}{3}(\nabla.\bar{v})\right)\right] + \frac{1}{r}\frac{\partial}{\partial r}\left[r\mu\left(\frac{\partial v_z}{\partial r}+\frac{\partial v_r}{\partial z}\right)\right]+(\rho-\rho_\infty)g \quad (2)$$

$$\frac{\partial}{\partial t}(\rho v_r)+\frac{1}{r}\frac{\partial}{\partial z}(r\rho v_z v_r)+\frac{1}{r}\frac{\partial}{\partial r}(r\rho v_r v_r) = -\frac{\partial p}{\partial r}+\frac{1}{r}\frac{\partial}{\partial z}\left[r\mu\left(\frac{\partial v_r}{\partial z}+\frac{\partial v_z}{\partial r}\right)\right] + \frac{1}{r}\frac{\partial}{\partial r}\left[r\mu\left(2\frac{\partial v_r}{\partial r}-\frac{2}{3}(\nabla.\bar{v})\right)\right]-2\mu\frac{v_r}{r^2}+\frac{2}{3}\frac{\mu}{r}(\nabla.\bar{v}) \quad (3)$$

where $(\nabla.\bar{v})=\frac{\partial v_z}{\partial z}+\frac{\partial v_r}{\partial r}+\frac{v_r}{r}$

$$\frac{\partial}{\partial t}(\rho Y)+\frac{\partial}{\partial z}(v_z\rho Y)+\frac{\partial}{\partial r}(v_r\rho Y) = \frac{\partial}{\partial z}\left(\rho D_b\frac{\partial Y}{\partial z}\right)+\frac{1}{r}\frac{\partial}{\partial r}\left(r\rho D_b\frac{\partial Y}{\partial r}\right) \quad (4)$$

Eq. (1) is the continuity equation and Eqs. (2) and (3) are, respectively, the axial and radial momentum conservation equations. Eq. (4) is the species mass conservation equation. The density was computed from the ideal gas law using local pressure and mixture composition (or molecular weight). The dynamic viscosity was computed using Wilke's mixture average formula (Bird et al., 1960) to account for local variations in the mixture composition. The mass diffusivity of helium into air (or air into helium) was taken as a constant value of 7.44e − 05 m^2/s (Geankoplis, 1972).

2.3. Boundary and initial conditions

Fig. 1 shows the computational domain whereby the left-side boundary represents the axis of symmetry. Domain sizes ranging from 10 d × 3 d (in axial and radial directions) to 50 d × 10 d were considered initially to evaluate the effect of the domain size on flow predictions. Based on this evaluation, the domain size of 15 d × 6 d was chosen for further analysis. The inlet boundary was placed at a distance of 1 d upstream from the jet exit plane. This was necessary to capture diffusion upstream of the jet exit observed in experimental studies (Cetegen and Kasper, 1996; Cetegen, 1997a; Pasumarthi and Agrawal, 2003) and back flow of air into the tube reported by Cetegen (1996, 1997a). At the tube inlet, the axial velocity profile was laminar and fully developed and the helium mole fraction was unity. No slip conditions were imposed on the inner and outer walls of the tube. The remaining boundaries were specified as open boundaries, whereby the normal flow gradients were zero. The initial conditions were zero axial and radial velocities and helium concentration throughout the interior domain.

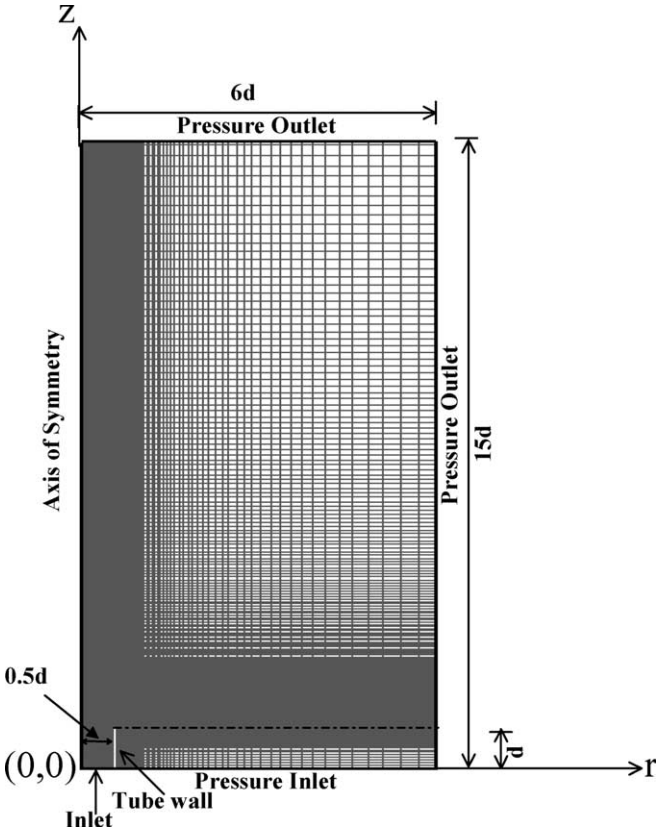

Fig. 1. Schematic of the computational domain.

2.4. Computational details

An orthogonal grid was generated by splitting the computational domain into five sub regions. The grid points in the radial direction were concentrated to resolve steep gradients in the flow oscillation region (see Fig. 1). The grid spacing was gradually increased in the axial direction. A single grid of one radian was used in the circumferential because of the axisymmetric nature of the problem. The governing equations were discretized using the finite volume approach (Fluent, 2005). The convective terms were discretized using the QUICK scheme and the pressure–velocity coupling was implemented using the SIMPLEC algorithm. The governing equations were solved in a segregated manner using an implicit, second-order time-dependent formulation. Sufficient time was allowed for the flow to achieve either periodic oscillations or steady conditions to ensure that the solution was independent of numerical disturbances and initial conditions.

2.5. Grid convergence and model validation

Computations with different grid sizes were performed to obtain grid independent solution. Trials were also

performed with different time steps to ensure that the solution was not affected by the time step. Based on these trials discussed briefly by Satti and Agrawal (2004), the grid with 270 axial and 110 radial nodes (270×110) and time step of 1.6 ms was chosen for further analysis. The computational model was validated for steady flow using concentration measurements of Shenoy et al. (1998). Fig. 2(a) shows an excellent agreement between computed and measured radial profiles of helium concentration at $z/d = 1.0$. The discrepancy in the center region is attributed to experimental errors introduced by the line of sight measurement technique used by Shenoy et al. (1998). Results in Fig. 2(a) prove that the model correctly simulated the flow structure of steady, low-density gas jets. The next step pertains to the verification of the model to predict flow oscillations in helium jets injected into air. Fig. 2(b) compares the computed and measured Strouhal numbers for a range of jet Richardson numbers. The measurements refer to the power law correlation of Hamins et al. (1992) and data taken from Cetegen and Kasper (1996). Again, an excellent agreement between computed and measured oscillation frequencies is reached, proving reliability of the model in predicting the global features of the oscillating flow.

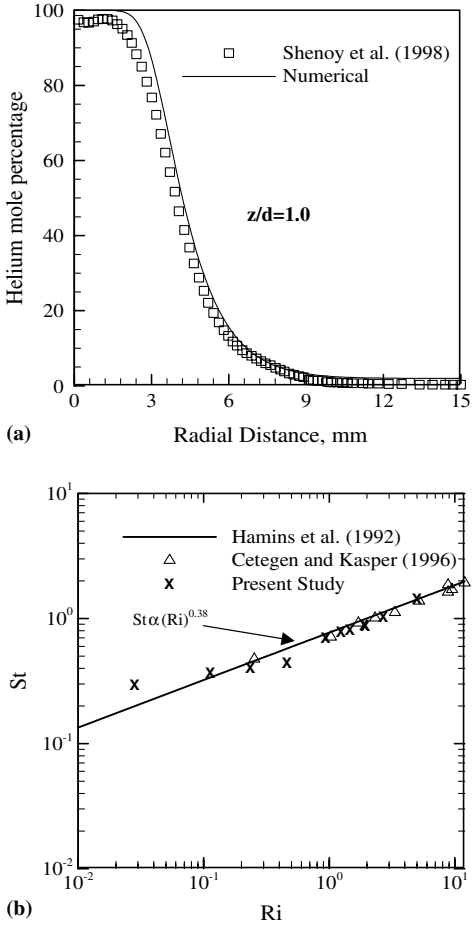

Fig. 2. (a) Experimental–numerical comparison of helium mole percentage profiles in a steady helium jet, $Re = 150$, $Ri = 0.07$, $d = 7.2$ mm. (b) Comparison between computed and measured Strouhal number versus jet Richardson number.

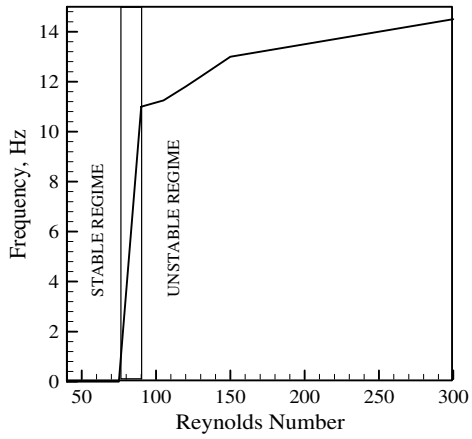

Fig. 3. Variation of oscillation frequency with jet Reynolds number for $d = 31.8$ mm.

3. Results and discussion

As observed by Hamins et al. (1992), a minimum jet exit velocity is required to initiate periodic flow oscillations. Previous studies have attributed unsteady flow oscillations to relative roles of diffusion and buoyant convection. Motivated by these ideas, computations were performed at several jet exit velocities (or jet Reynolds numbers) to demarcate the steady and unsteady flow regimes. As explained previously, no external perturbations were introduced and computations were performed for sufficiently long time such that the flow reached either steady conditions or periodic oscillations with no change between consecutive cycles. Fig. 3 plots the flow oscillation frequency versus jet Reynolds number. The flow was steady for $Re < 70$, and the change from steady to oscillatory state occurred approximately at $Re = 90$ or $U_j = 0.33$ m/s. The computed velocity required to initiate oscillations matches well with the measured velocity of approximately 0.3 m/s reported by Hamins et al. (1992) for $d = 25.0$ mm. Such agreement is fortuitous and further substantiates the effectiveness of the present model. The oscillation frequency increased gradually from 11 Hz for $Re = 90$ to 14.5 Hz for $Re = 300$. Next, the detailed flow structure is examined for four test cases: two cases pertaining to the steady flow and two cases to represent the oscillating flow. The operating conditions for these test cases are summarized in Table 1.

Table 1
Summary of test conditions

Case	d (mm)	U_j (m/s)	Re	Ri	f (Hz)
1	31.8	0.15	40	85	Steady
2	31.8	0.27	70	30	Steady
3	31.8	0.34	90	17	11
4	31.8	0.56	150	6.4	13

3.1. Global flow characteristics

The flow structure of the low-density gas jet is influenced by the jet Reynolds number. Fig. 4 shows velocity vectors in the near-field ($z/d = -1.0$ to 2.0, where $z/d = 0.0$ represents the tube exit plane) for different jet Reynolds numbers. The vectors are drawn at selected grid locations to prevent over-crowding. For $Re = 40$, the velocity vectors in Fig. 4(a) show strong curvature inside the jet tube. Evidently, the jet core accelerates by buoyant convection of helium. Concurrently, the ambient fluid settles inside the tube in a region adjacent to the wall, because the momentum of the light weight helium is insufficient to displace the heavier ambient fluid. This phenomenon of back flow of air upstream of the jet exit was reported by Cetegen and Kasper (1996), who utilized a flat stainless steel screen at the tube exit to enforce flow uniformity. For $Re = 70$, the back flow of the ambient fluid inside the jet tube is insignificant because of the higher momentum of the jet (see Fig. 4(b)).

For $Re = 90$, the velocity vectors in Fig. 4(c) show a recirculation region at $z/d = 0.3$, indicating that the critical velocity to initiate flow oscillations has surpassed. Fig. 4(c) pertains to the cyclic phase at the onset of the instability characterized by entrainment of ambient fluid into the jet core. Similar features of the vortex are also observed in Fig. 4(d) for $Re = 150$. However, the vortex core is located closer to the jet axis at the lower jet Reynolds number, i.e., $r/d = 0.44$ for $Re = 90$ compared to $r/d = 0.56$ for $Re = 150$. Moreover, the width of the vortex is greater for $Re = 150$ compared to $Re = 90$.

The jet half width (or radius) is an important parameter to quantify radial growth of the jet in the streamwise direction. Fig. 5 plots the normalized jet half radius ($r_{1/2}/d$) at several axial locations, computed using axial velocity and helium concentration profiles. The jet half radius ($r_{1/2}$) is defined as the radial location where the axial velocity or helium concentration is half of that at the jet center ($r/d = 0.0$). In case of the oscillating flow, the time-averaged profiles were used to determine the jet half radius. Fig. 5 reveals several unique features of low-density gas jets. First, the jet half radius is the highest near the tube exit and it decreases in the flow direction for all cases. This trend signifying contraction of the jet in the flow direction is opposite to the radial growth observed in constant density jets. The contraction of the jet is attributed to buoyant acceleration of the low-density jet fluid, which promotes scalar mixing by entraining ambient fluid into the jet core. For all cases, the jet half radius based on axial velocity profiles is smaller than the scalar jet half radius. Fig. 5 displays another unique feature of low-density gas jets; the jet half radius increases with increasing jet Reynolds number, a trend opposite of constant density gas jets. The jet is wider at higher jet Reynolds numbers because the contraction of the jet by buoyant acceleration of low-density jet fluid is less prominent. Overall, results show significant differences in the flow structure of low-density jets compared to constant density jets. Next, detailed flow characteristics of steady and oscillating jets are examined in the following sections.

3.2. Steady jet

In this section, structural details of the steady flow are discussed using radial profiles of axial velocity and helium concentration. These profiles are presented at several axial

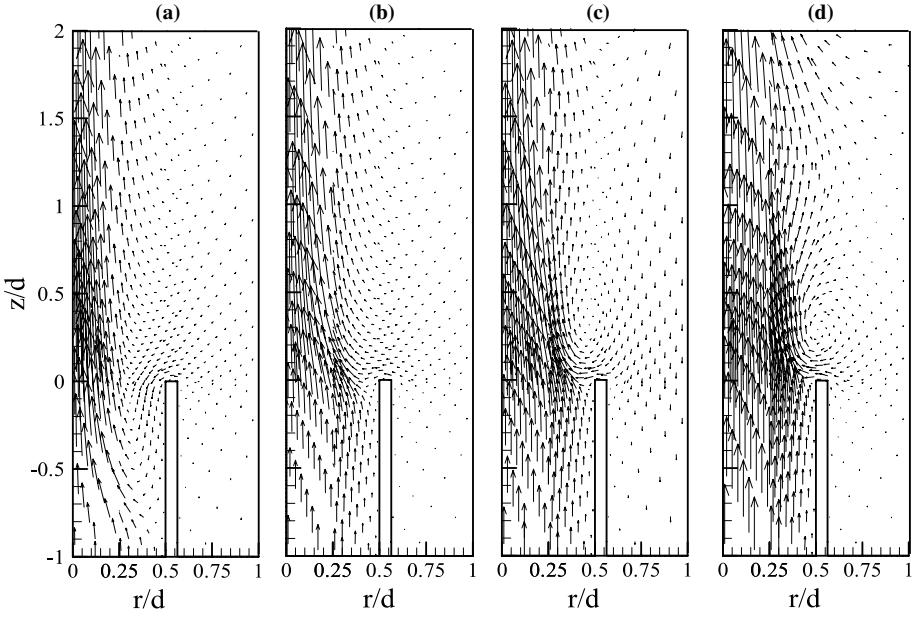

Fig. 4. Velocity vectors for $d = 31.8$ mm. (a) $Re = 40$, $Ri = 85$ (steady) (b) $Re = 70$, $Ri = 30$ (steady) (c) $Re = 90$, $Ri = 17$ (oscillating) (d) $Re = 150$, $Ri = 6.4$ (oscillating).

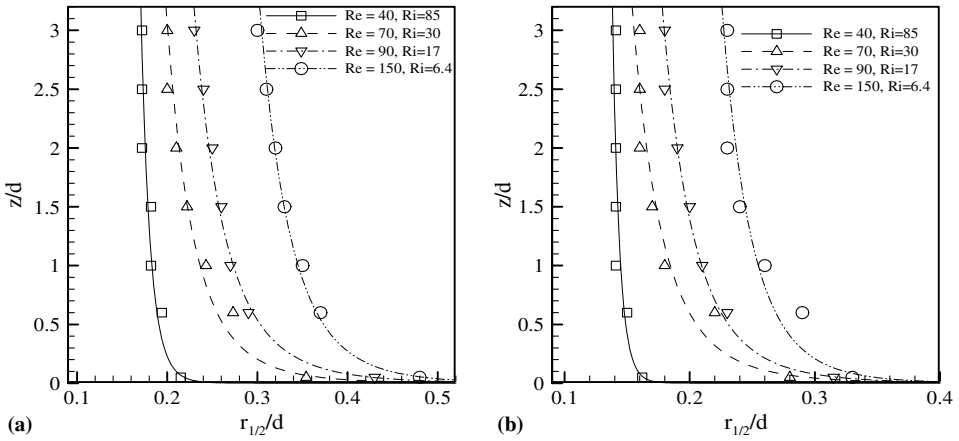

Fig. 5. Jet half radius in the flow direction based on (a) helium concentration and (b) axial velocity profiles.

locations inside the tube and near the jet exit to highlight interactions between velocity and concentration fields.

3.2.1. Re = 40

Fig. 6 reveals major changes in profiles inside and downstream of the tube for $Re = 40$. For example, the axial velocity at the jet center ($r/d = 0.0$) increased by nearly a factor of four within the jet tube; from 0.3 m/s at the injection plane ($z/d = -1.0$) to approximately 1.2 m/s near the tube exit plane ($z/d = -0.25$). Acceleration in the jet core region ($r/d < 0.25$) is accompanied with deceleration in the wall region ($r/d > 0.25$). Moreover, the axial velocity profiles depict flow reversal between $r/d = 0.32$ and tube wall for $z/d > -0.50$. This unusual behavior is attributed to the sinking of the heavier ambient fluid (by gravity) above the lighter jet fluid in the low-momentum

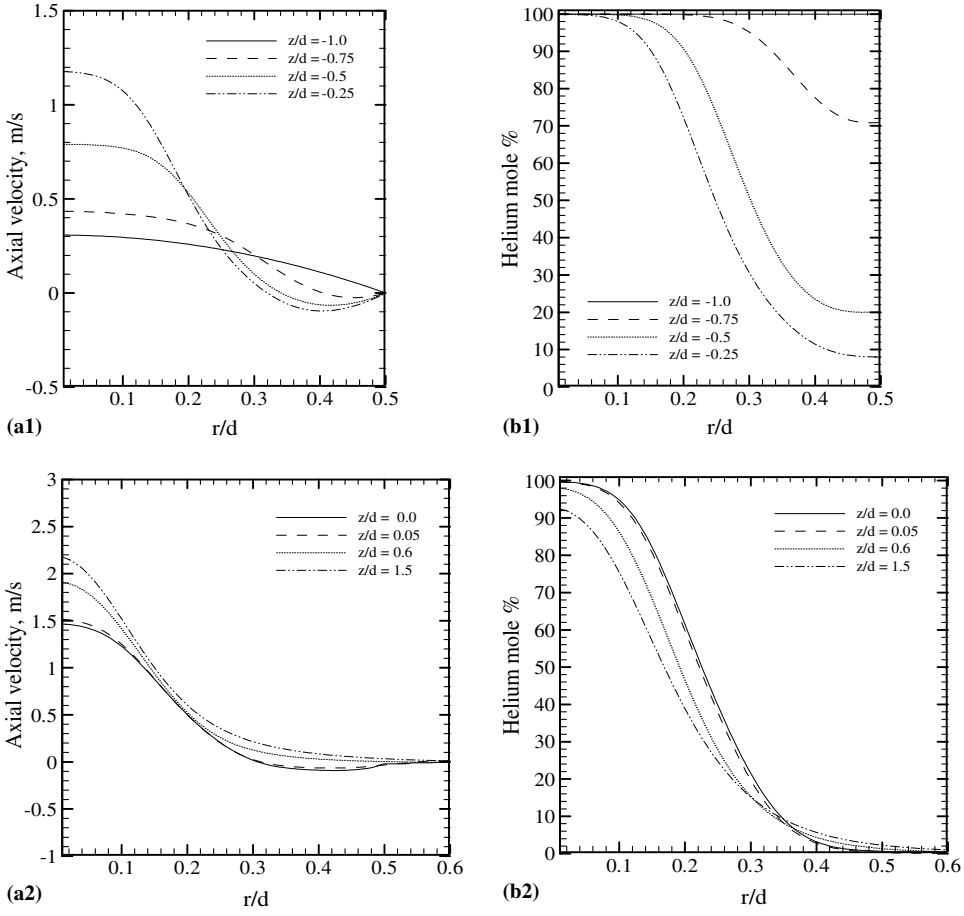

Fig. 6. Profiles of axial velocity (a1, a2) and helium mole percentage (b1, b2), $Re = 40$, $Ri = 85$, $d = 31.8$ mm.

region adjacent to the wall. In contrast, buoyancy accelerates the jet core region with sufficient momentum to displace the ambient fluid above it. Helium concentration profiles in Fig. 6(b1) show vigorous mixing of jet and ambient fluids inside the tube. For example, air has reached up to $r/d = 0.25$ at $z/d = -0.75$ and almost to the jet center ($r/d = 0.0$) at $z/d = -0.25$. The mixing of the jet and ambient fluids by buoyant convection and molecular diffusion produces a stratified density shear layer at the tube exit. Essentially, such stratification would hinder entrainment of the ambient fluid into the jet core region to prevent the formation of the toroidal vortex downstream of the tube exit.

The development of axial velocity and helium concentration profiles downstream of the tube exit is depicted in Fig. 6(a2)–(b2) for $Re = 40$. Results show that the flow at all radial locations accelerates in the streamwise direction and positive axial velocity is reached at $z/d = 0.6$. The axial velocity at the center point increases from 1.50 m/s at $z/d = 0.0$ to 2.2 m/s at $z/d = 1.5$, representing only moderate flow acceleration compared to that inside the tube. The helium concentration profiles in Fig. 6(b2) show presence of air in much of the jet core region at the tube exit. Helium concentration at the center point reduces to 98% at $z/d = 0.6$ and to 92% at $z/d = 1.5$, indicating gradual mixing of fluids downstream of the tube exit.

3.2.2. Re = 70

Fig. 7 shows axial velocity and helium concentration profiles for $Re = 70$. The profiles at $z/d = -0.25$ are nearly identical to those at the injection plane $z/d = -1.0$. At the jet center, the axial velocity increases from 0.54 m/s at the injection plane to 0.68 m/s near the tube exit ($z/d = -0.05$), with much of the change occurring after $z/d = -0.25$. The reverse flow inside the tube is confined to a narrow region, $r/d = 0.45$–0.50, near the tube exit or $z/d = -0.05$. Pure helium is present up to $r/d = 0.33$ at $z/d = -0.10$ and up to $r/d = 0.30$ at $z/d = -0.05$. Again, mixing inside the tube produces a stratified density shear layer at the tube exit. Fig. 7(a2) shows significant acceleration of the jet core region downstream of the tube exit. For example, the axial velocity at the center point increases from 0.72 m/s at the tube exit ($z/d = 0.0$) to 2.35 m/s at $z/d = 1.5$, indicating a more than threefold increase. Helium concentration profiles in Fig. 7(b2) show vigorous mixing by entrainment/diffusion of ambient fluid into the jet core region. Results show similarities in the flow structure for the two test cases, although mixing and buoyant acceleration are prominent

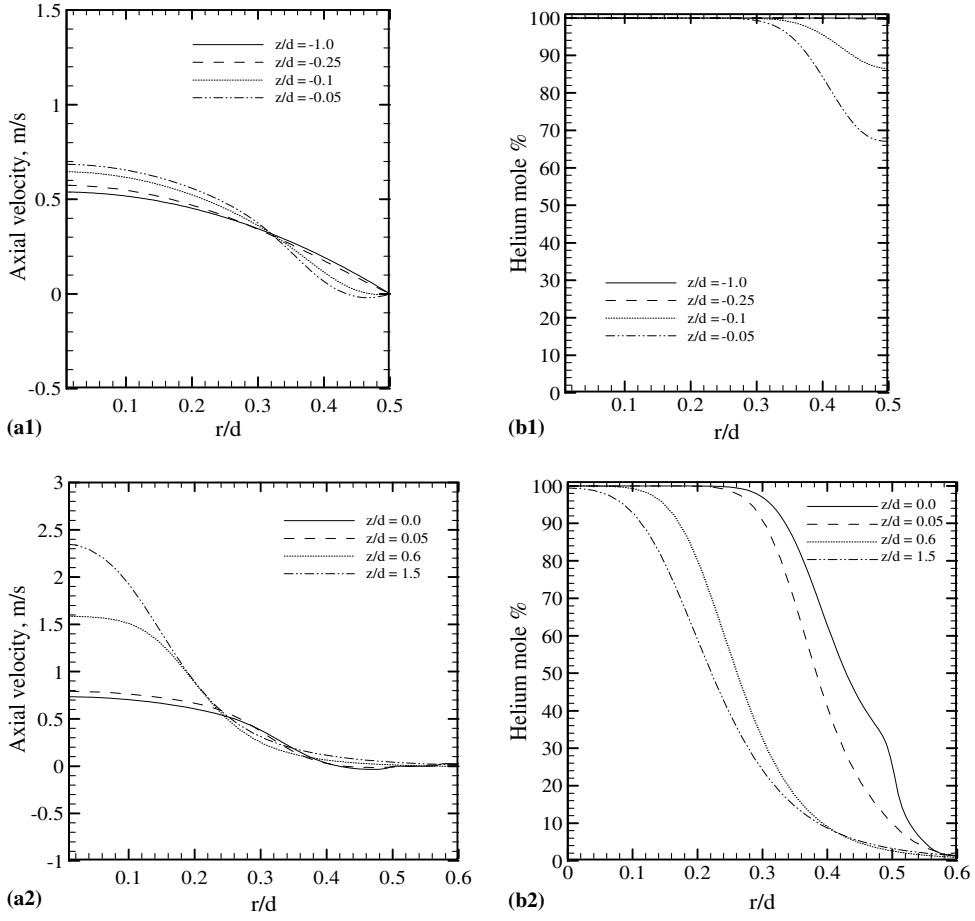

Fig. 7. Profiles of axial velocity (a1, a2) and helium mole percentage (b1, b2), $Re = 70$, $Ri = 30$, $d = 31.8$ mm.

inside the tube for $Re = 40$ and downstream of the tube exit for $Re = 70$.

3.3. Oscillating jet

In this section, we examine the dynamics of the oscillating jet including interactions between velocity and concentration fields, and instantaneous and time-averaged flow structure.

3.3.1. Simultaneous visualization of velocity and concentration fields

Fig. 8 shows velocity vectors superimposed with contours of helium mole percentage during an oscillation cycle for $Re = 150$. The first plot for $t = 0.0$ ms reveals a small flow recirculation region (vortical motion) described by the clockwise velocity vectors near $r/d = 0.5$ (the vortex core is indicated by a black dot in the figure). This phase marks the initiation of the instability leading to a larger recirculation zone at $t = 16.0$ ms, where the vortex core is located at $z/d = 0.40$. The vortex formation is associated with buoyant acceleration of the jet fluid causing the jet core to contract, as indicated by the strong concave curvature of the concentration contours between $z/d = 0.0$ and 0.30. Buoyant acceleration entrains the ambient fluid into the jet core, as indicated by radially oriented velocity vectors upstream of the vortex core. At $t = 32.0$ and 48.1 ms, we observe the vortex region growing in size and intensity. Fig. 8 shows that the vortex gains momentum by interacting with the jet core, whereby velocity vectors downstream of the vortex core have higher magnitudes than those upstream. At $t = 64.1$ ms, the vortex convects downstream and it has contaminated much of the jet core region. As the straining effect of the vortex diminishes, the jet expands near the tube exit to initiate another vortex at $t = 80.1$ ms to repeat the oscillation cycle. Similar unsteady features characterized by formation and propagation of vortical structures were observed for $Re = 90$, although those results are not presented here for brevity.

These observations of the flow structure are summarized as follows: As the helium exits the tube, the jet core accelerates by buoyancy and contracts to conserve the mass. The contraction of the jet results in entrainment of the ambient fluid to form a toroidal vortex which grows in size, accelerates, and convects downstream. As the vortex convects downstream, it penetrates closer to the centerline to contaminate the jet core. In the immediate downstream region of the vortex, the jet core decelerates owing to the transfer of the momentum to the vortex. With the vortex moving away from the tube, the jet expands again near the tube exit. Subsequently, buoyancy manifests to accelerate the jet core to form a toroidal vortex to repeat the oscillation cycle. These observations are consistent with velocity measurements of Cetegen (1997b) and concentration measurements of Pasumarthi and Agrawal (2003) for helium jets in air.

3.3.2. Instantaneous flow structure

Instantaneous profiles of axial velocity and helium concentration were obtained to depict the periodicity and streamwise development of the flow structure. Fig. 9 shows

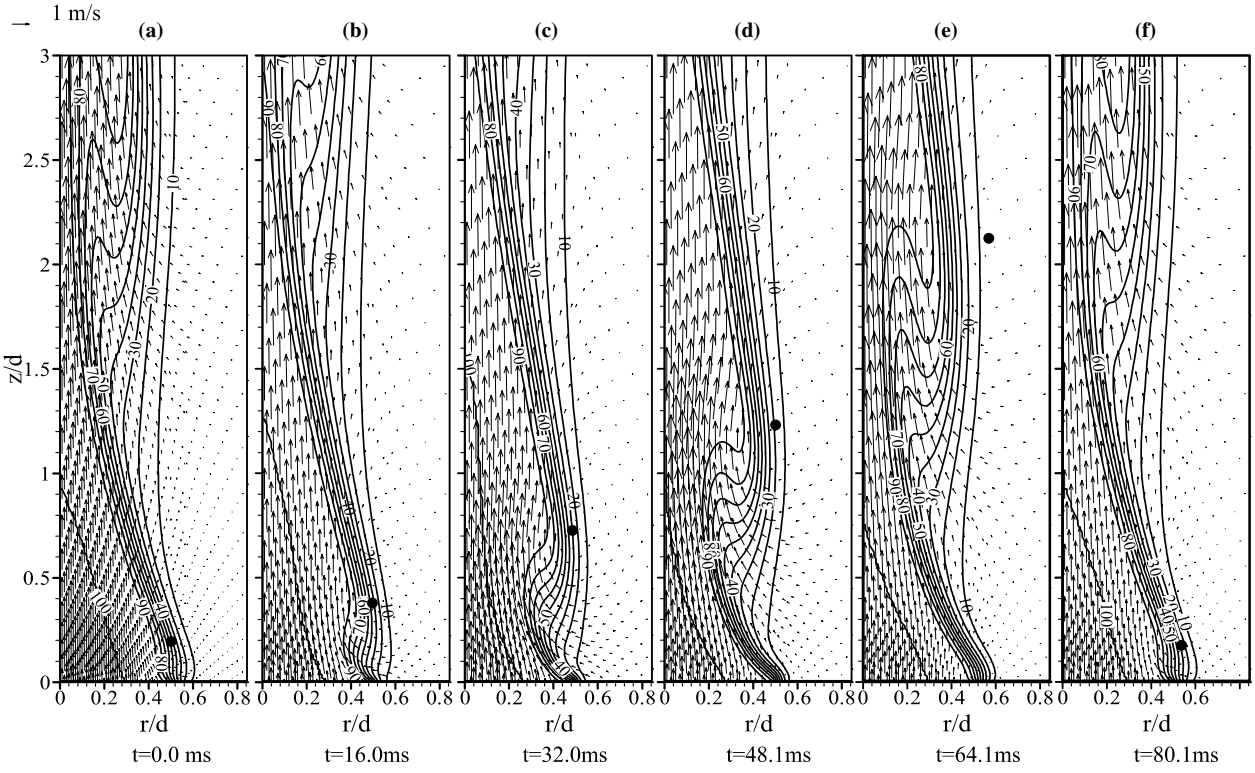

Fig. 8. Velocity vectors superimposed by contours of helium mole percentage during an oscillation cycle for $Re = 150$, $Ri = 6.4$, $d = 31.8$ mm.

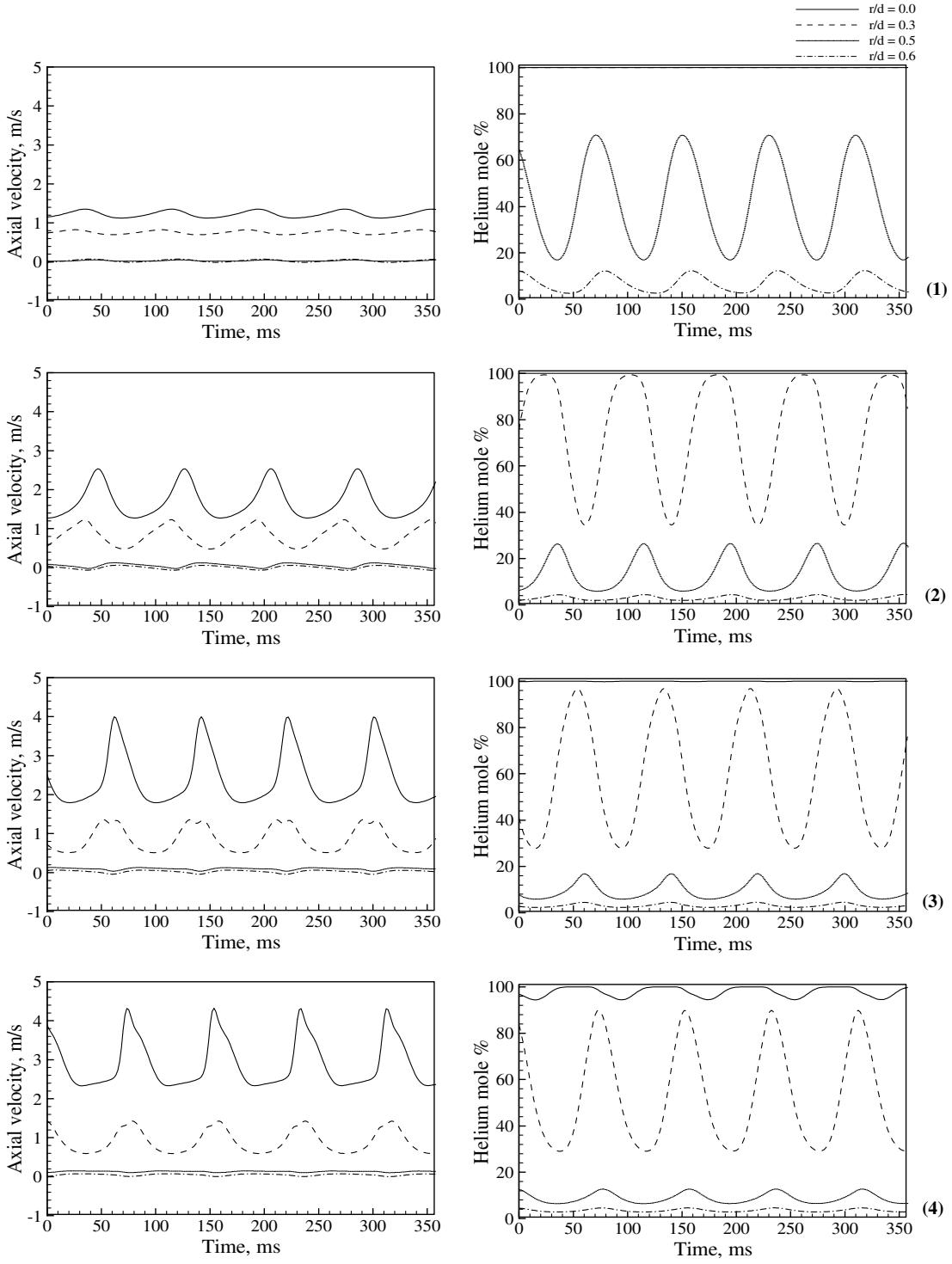

Fig. 9. Time trace plots of axial velocity and helium mole percentage at different radial locations for $Re = 150$, $Ri = 6.4$, $d = 31.8$ mm. (1) $z/d = 0.05$ (2) $z/d = 0.6$ (3) $z/d = 1.5$ (4) $z/d = 2.5$.

these plots at selected axial and radial locations for a brief period for $Re = 150$. Results show highly periodic oscillations throughout the flow field. Based on the time lag between two consecutive crests/troughs, oscillation frequency of 13 Hz was obtained at all locations, which agrees with experiments showing self-excited global oscillations in the flow field.

Fig. 9 shows that near the jet exit at $z/d = 0.05$, pure helium is present in the core region ($r/d = 0.0$ and 0.3) at all times. However, large concentration fluctuations are observed in the shear layer region ($r/d = 0.5$) with helium mole percentage ranging from 16% to 70%. The concentration profile at $r/d = 0.6$ indicates that the helium has diffused beyond the tube wall. The axial velocity profiles at

$z/d = 0.05$ show periodic oscillations at all radial locations, with the amplitude of oscillations decreasing in the radial direction. Further downstream at $z/d = 0.6$, the jet core at $r/d = 0.3$ has been contaminated by air with helium concentration varying between 35% and 100%. A somewhat flattened peak in the concentration profile indicates that pure helium is present only for a brief interval during the oscillation cycle. At $r/d = 0.5$, the helium concentration has decreased to between 10% and 25% indicating increased penetration of air into the jet core at downstream locations. The helium concentration at $r/d = 0.6$ has also reduced to between 2% and 6% because the jet core is contracting instead of growing outwards. The axial velocity profiles show an increase of velocity in the jet core ($r/d = 0.0$ and 0.3) attributed to buoyant acceleration. The peak values at the jet center are 1.4 and 2.6 m/s, respectively, at $z/d = 0.05$ and 0.60. The axial velocity fluctuations are highest at the centerline, where the axial velocity is also the highest. The axial velocity and its oscillation amplitude are small at $r/d = 0.5$ and 0.6, a region coinciding with the vortex core.

At $z/d = 1.5$, pure helium is present at the jet center for all times. However, helium concentration has reduced to between 28% and 96% at $r/d = 0.3$ and 8 and 16% at $r/d = 0.5$, by entrainment of air into the jet core. Axial velocity profiles show buoyant acceleration of the jet core with peak axial velocity rising to 4.0 m/s at the centerline. The slope of the axial velocity profile at $r/d = 0.0$ shows a period of slow acceleration followed by rapid acceleration and deceleration phases. Note that the jet flow accelerates by buoyancy and decelerates by momentum transfer to the surrounding vortex. Finally, at $z/d = 2.4$, the ambient fluid has reached the jet centerline where the helium concentration varies between 94% and 100%. A flattened peak at $r/d = 0.0$ indicates that pure helium is present during about half of the oscillation cycle. The concentration levels at $r/d = 0.3$ and 0.5 have decreased because of the mixing of the helium with air. Note that the entrainment of the ambient fluid has prevented the helium to diffuse radially outwards, except near the tube exit. The axial velocity profiles at the jet centerline ($r/d = 0.0$) agree qualitatively with those obtained experimentally by Subbarao and Cantwell (1992) in buoyant helium jets with co-flow of air.

3.3.3. Mean and RMS flow structure

Fig. 10 shows radial profiles of mean and root-mean-square (RMS) axial velocity and helium concentration at various axial planes for $Re = 90$ and 150. The mean axial velocity profile at $z/d = 0.05$ is parabolic, representing fully developed laminar flow at the tube exit. For both cases, the mean axial velocity increases between $r/d = 0.0$ and 0.28 in the flow direction, signifying buoyant acceleration of the jet core. The increase is the highest at the jet center where the mean axial velocity is also the highest. The RMS axial velocity fluctuations are highest at the jet centerline owing to periodic acceleration of the jet core by buoyancy and deceleration by the passage of the vortex. For $Re = 90$, the peak RMS axial velocity of 0.05 m/s at $z/d = 0.05$ increases to 0.28 m/s at $z/d = 0.6$ and to 0.4 m/s at $z/d = 1.5$. For $Re = 150$, the peak RMS axial velocity of 0.05 m/s at $z/d = 0.05$ increases to 0.45 m/s at $z/d = 0.6$ and to 0.7 m/s at $z/d = 1.5$. These observations of mean and RMS axial velocity profiles are consistent with velocity measurements of Subbarao and Cantwell (1992).

The concentration profiles near the tube exit ($z/d = 0.05$) show that the helium has reached beyond $r/d = 0.65$ and pure helium is present only up to $r/d = 0.3$ for $Re = 90$ and to $r/d = 0.38$ for $Re = 150$. At $z/d = 0.6$, mixing has caused mean helium concentration at $r/d = 0.5$ to decrease to 5% for $Re = 90$ and to 15% for $Re = 150$. The concentration profile for $Re = 150$ shows an inflection point at $z/d = 1.5$ because of the vortex interacting with the jet core. Note that entrainment by the vortex has restricted the jet from spreading outwards. Overall, the mean flow structure depicts greater contamination of the jet core for $Re = 90$ compared to $Re = 150$ because of the inward movement of the vortex for the latter.

The RMS concentration profiles reveal larger fluctuations at higher jet Reynolds number. For $Re = 90$, the peak RMS concentration is between 15% and 20% at all axial locations. For $Re = 150$, the peak RMS concentration increases from 20% at $z/d = 0.05$ to approximately 25% at $z/d = 0.6$ and 1.5. The location of the peak concentration shifts inwards in the flow direction. Concentration fluctuations confined to the wake region ($0.4 < r/d < 0.6$) near the jet exit broaden in the axial direction and contaminate most of the flow at $z/d = 1.5$. These observations agree qualitatively with experimental results presented by Pasumarthi and Agrawal (2003).

3.4. Instability mechanism

The above results highlighted interesting features of low-density gas jets in both steady and oscillating flow regimes. In particular, it was shown that a minimum jet exit velocity is required to initiate flow oscillations, a phenomenon reported experimentally by Hamins et al. (1992). In our discussion, we alluded that a minimum jet exit velocity was needed to prevent stratification of the concentration shear layer. The adjacent fluid elements in a stratified shear layer will accelerate gradually with respect to each other because buoyancy is proportional to density. However, a sharp interface in the concentration shear layer would cause the low-density fluid to accelerate rapidly to entrain the high-density fluid. The rates of acceleration and entrainment will determine the formation of the toroidal vortex. In this study, the concentration shear layer was stratified by ambient fluid settling inside the tube at low Re. Thus, the entrainment caused by the accelerating jet core was not sufficient to form a vortex downstream of the tube exit. However, the sharp interface at higher Reynolds numbers accentuated entrainment of ambient fluid into the jet core to create a vortex and hence, periodic oscillations in the flow field. This explanation is supported by Fig. 11 showing

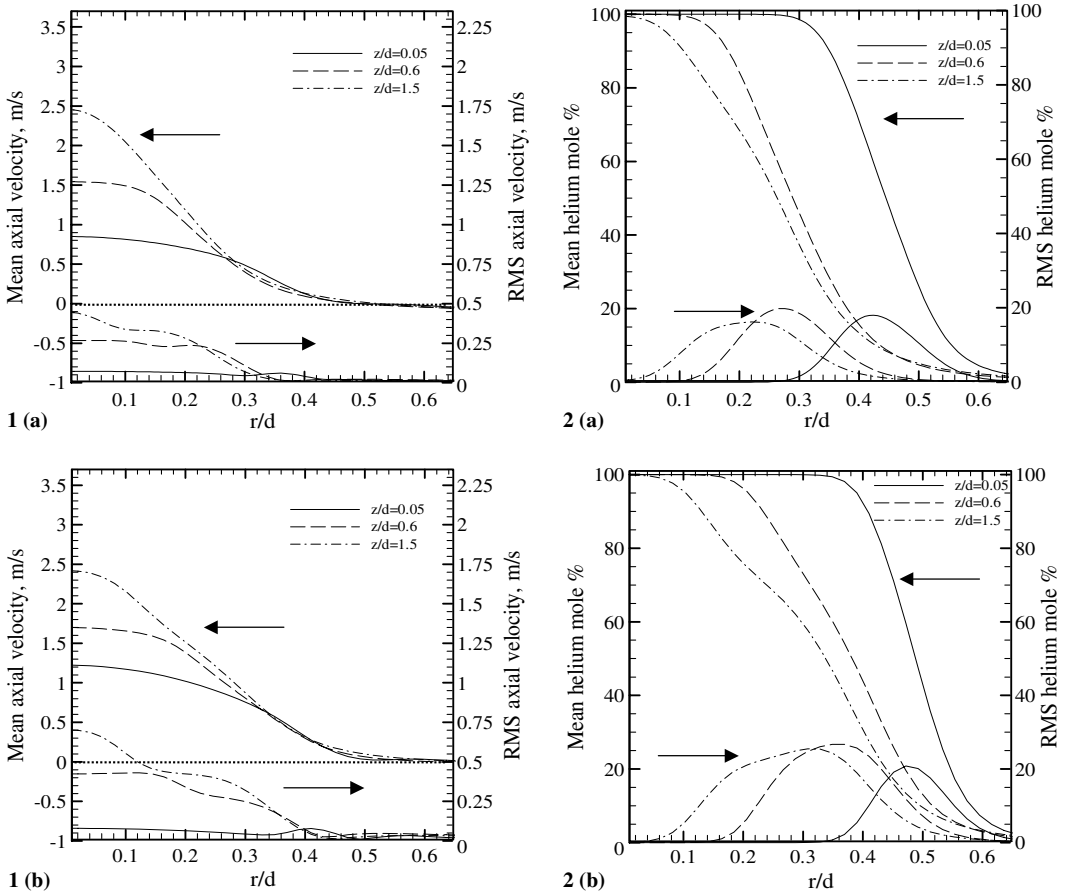

Fig. 10. Profiles of mean and RMS (1) axial velocity and (2) helium mole percentage, (a) $Re = 90$, $Ri = 17$, $d = 31.8$ mm. (b) $Re = 150$, $Ri = 6.4$, $d = 31.8$ mm.

radial profiles of density gradient in the radial direction for all cases at $z/d = 0.3$. Results show that the peak density gradient increased with increasing jet Reynolds number, indicating a shear layer with sharper density interface at higher *Re*. The location of the peak density gradient shifted towards the tube wall ($r/d = 0.5$) with an increase in the jet Reynolds number.

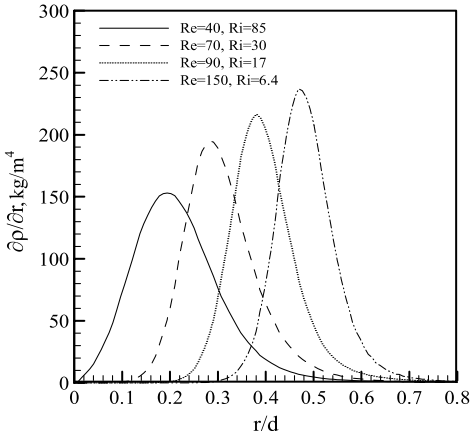

Fig. 11. Radial profiles of density gradient in radial direction at $z/d = 0.3$.

4. Conclusions

Steady and oscillating flow structure of helium jets injected into quiescent air was simulated using computational fluid dynamics. Comparison with experimental data revealed that the computational model was effective in predicting complex structural details including the change from steady to oscillating flow as the jet Reynolds number was increased. Important results of the study are summarized in the following:

- The flow was steady at low jet Reynolds numbers of 40 and 90. The lighter jet fluid in the core region accelerated by buoyancy, while the heavier ambient fluid settled adjacent to the tube wall. The backflow of ambient fluid inside the tube was significant at the lower jet Reynolds number. The mixing of the jet and ambient fluids inside the tube resulted in a stratified shear layer at the tube exit. Downstream of the tube exit, the mixing was dominated by the entrainment of the ambient fluid into the accelerating jet core.
- Self-excited periodic oscillations at a unique frequency were observed throughout the near-field at jet Reynolds numbers of 90 and 150. Flow oscillations were caused by

buoyant acceleration of the jet core entraining ambient fluid to form a toroidal vortex. The vortex interacted with the jet core, while growing in size, accelerating, and convecting downstream. The vortex path was oriented more towards the jet center at the higher jet Reynolds number.

- The jet half radius decreased in the flow direction for both steady and oscillating flows. This trend indicating contraction of the jet in the flow direction (because of buoyant acceleration) is opposite of constant density gas jets. Furthermore, in contrast to constant density jets, the jet half radius increased with increase in the jet Reynolds number. At low jet Reynolds numbers, the radial expansion of the jet was suppressed by buoyant acceleration, an effect that became less prominent at higher jet Reynolds numbers.
- The onset of the instability was related to the shape of the concentration (or density) shear layer near the tube exit. The instability was suppressed in a stratified density shear layer. However, flow oscillations occurred if the density shear layer contained a sharp interface.

Acknowledgment

This work was supported by NASA's Office of Biological and Physical Research under Grant NNC04GA22G.

References

Bird, R.B., Stewart, W.E., Lightfoot, E.N., 1960. Transport Phenomena, first ed. Wiley, New York.

Cetegen, B.M., Ahmed, T.A., 1993. Experiments on the periodic instability of buoyant plumes and pool fires. Combustion and Flame 93, 157–184.

Cetegen, B.M., Kasper, K.D., 1996. Experiments on the oscillatory behavior of buoyant plumes of helium and helium–air mixtures. Physics of Fluids 8 (11), 2974–2984.

Cetegen, B.M., 1997a. Behavior of naturally unstable and periodically forced axisymmetric buoyant plumes of helium and helium–air mixtures. Physics of Fluids 9 (12), 3742–3753.

Cetegen, B.M., 1997b. Measurements of instantaneous velocity field of a non-reacting pulsating buoyant plume by particle image velocimetry. Combustion Science and Technology 123 (1–6), 377–387.

Dai, Z., Tseng, L.K., Faeth, G.M., 1994. Structure of round, fully developed, buoyant turbulent plumes. Journal of Heat Transfer 116 (2), 409–417.

Dehmani, L., Kim-Son, Doan, Gbahoue, L., 1996. Turbulent structure of an axisymmetric plume penetrating strong density stratification. International Journal of Heat and Fluid Flow 17 (5), 452–459.

Fay, J.A., 1973. Buoyant plumes and wakes. Annual Review of Fluid Mechanics 5, 151–160.

Fluent 6 User's guide, FLUENT Inc., Lebanon, NH, 2005.

Geankoplis, C.J., 1972. Mass Transport Phenomena. Holt, Rinehart and Winston, New York.

Gebhart, B., 1973. Instability, transition, and turbulence in buoyancy-induced flows. Annual Review of Fluid Mechanics 5, 213–246.

Hamins, A., Yang, J.C., Kashiwagi, T., 1992. An experimental investigation of the pulsating frequency of flames. Proceedings of the Combustion Institute 24, 1695–1705.

Lai, J.C.S., 1984. Unsteady effects in mechanically excited turbulent plane jets. International Journal of Heat and Fluid Flow 5 (4), 215–221.

List, E.J., 1982. Turbulent jets and plumes. Annual Review of Fluid Mechanics 14, 189–212.

Mell, W.E., McGrattan, K.B., Baum, H.R., 1996. Numerical simulation of combustion in fire plumes. Proceedings of the Combustion Institute 26, 1523–1530.

Mollendorf, J.C., Gebhart, B., 1973. An experimental and numerical study of the viscous stability of a round laminar vertical jet with and without thermal buoyancy for symmetric and asymmetric disturbances. Journal of Fluid Mechanics 61, 367–399.

Panchapakesan, N.R., Lumley, J.L., 1993. Turbulence measurements in axisymmetric jets of air and helium. Part 2. Helium jet. Journal of Fluid Mechanics 246, 225–248.

Papanicolaou, P.A., List, E.J., 1988. Investigations of round vertical turbulent buoyant jets. Journal of Fluid Mechanics 195, 342–391.

Pasumarthi, K.S., Agrawal, A.K., 2003. Schlieren measurements and analysis of concentration field in self-excited helium jets. Physics of Fluids 15 (12), 3683–3692.

Pera, L., Gebhart, B., 1963. On the stability of laminar plumes: some numerical solutions and experiments. International Journal of Heat and Mass Transfer 14, 597–606.

Richards, C.D., Pitts, W.M., 1993. Global density effects on the self-preservation behavior of turbulent free jets. Journal of Fluid Mechanics 254, 417–435.

Rodi, W., 1982. Turbulent buoyant jets and plumes. International Journal of Heat and Fluid Flow 3 (4), 194.

Satti, R.P., Agrawal, A.K., 2004. Numerical analysis of flow evolution in a helium jet injected into ambient air. ASME Heat Transfer/Fluids Engineering Summer Conference, HT-FED2004-56811.

Shenoy, A.K., Agrawal, A.K., Gollahalli, S.R., 1998. Quantitative evaluation of flow computations by rainbow schlieren deflectometry. AIAA Journal 36, 1953–1960.

Soteriou, M.C., Dong, Y., Cetegen, B.M., 2002. Lagrangian simulation of the unsteady near field dynamics of planar buoyant plumes. Physics of Fluids 14 (9), 3118–3140.

Subbarao, E.R., Cantwell, B.J., 1992. Investigation of a co-flowing buoyant jet: experiments on the effects of Reynolds number and Richardson number. Journal of Fluid Mechanics 245, 69–90.

Tenner, A.R., Gebhart, B., 1971. Laminar and axisymmetric vertical jets in a stably stratified environment. International Journal of Heat and Mass Transfer 14 (12), 2051–2062.

Yep, T.W., Agrawal, A.K., Griffin, D.W., 2003. Gravitational effects on near field flow structure of low density gas jets. AIAA Journal 41, 1973–1979.